

Field Effect Enhanced Hydrogen Evolution Reaction of MoS₂ Nanosheets

Junhui Wang, Mengyu Yan,* Kangning Zhao, Xiaobin Liao, Peiyao Wang, Xuelei Pan, Wei Yang, and Liqiang Mai*

H₂ has been considered as a promising energy carrier for future energy technologies due to its high energy density and being environmentally friendly.^[1–4] In view of this, the production of hydrogen needs a highly-efficient and economical way to meet the increasing demand of clean energy. Water splitting, as a well-known way for H₂ production, has attracted attention for the advantages of non-pollutants and abundant sources.^[5,6] Water splitting includes the hydrogen evolution reaction (HER) and the oxygen evolution reaction, and both of them need catalysts to reduce the electrochemical overpotential.^[7–11] Generally speaking, the HER process consists of multiple reaction steps. In the acid electrolyte, the main steps can be described succinctly as a hydronium cation (H₃O⁺) adsorbed on a catalytic active site and coupled with an electron to form a hydrogen atom. There are two probable mechanisms to gain and eventually release a hydrogen molecule (H₂) from the active sites: (1) two hydrogen atoms combine directly; (2) a hydrogen atom captures an electron and a H₃O⁺ ion simultaneously.^[7,12,13] So a high-performance HER electrocatalyst should exhibit fast electron transfer, large density of catalytic active sites, and appropriate Gibbs free energy of adsorbed atomic hydrogen. Pt-group metals, which can meet the above requirements, are an excellent catalyst for HER, while their practical applications are limited by the rare reserve on the earth.^[14,15] Thus, it is imperative to investigate high-performance HER electrocatalyst with low costs.

Among those, theoretical calculation has proven that molybdenum disulfide (MoS₂) possesses an adequate Gibbs free energy of adsorbed atomic hydrogen, and it has the merit of element abundance; thus MoS₂ is regarded as a promising alternative of Pt.^[16–19] However, it is reported that the MoS₂ catalytic activity is hindered by the less number of thermodynamically unstable Mo edges (act as the active sites) and poor conductivity of the catalyst.^[20–22] Many means have been developed and utilized to improve the catalytic performance

of MoS₂,^[23,24] such as morphology and structure control to expose more active sites,^[25–28] constructing defects as active sites^[29–32] and compositing with other materials to accelerate electron transport speed.^[33–39] Recent work by Chhowalla and co-workers^[40] has reported that reducing contact resistance between the Au electrode and the catalyst can activate the intrinsic catalytic properties of basal plane of 2H MoS₂ by facilitating electron injection to the active sites. From previous research of MoS₂ transistor, it has been found that the electric field effect can simultaneously reduce the contact resistance and sheet resistance of MoS₂ materials to gain a faster electron transfer speed.^[41,42] Thus a better catalysis of MoS₂ for HER can be expected with the application of field effect.

Herein, we have successfully fabricated a field-tuned HER device with an individual MoS₂ nanosheet to explore the impact of field effect on catalysis. The catalytic property of MoS₂ nanosheet is clearly and dramatically improved with the addition of an electric field. The lowest overpotential of current density 100 mA μm⁻² could reach 38 mV and the value of Tafel slope at the back gate voltage of 5 V has fallen to half to that of no electric field. The inspirational result demonstrates that the field effect is a promising strategy to enhance the catalytic performance of MoS₂ for HER with lower channel resistance and faster charge transfer.

The fabrication process of a field-tuned individual MoS₂ nanosheet based HER device is schematically illustrated in **Figure 1** and **Figure S1** in the Supporting Information.^[43,44] A suitable size silicon wafer (with 300 nm dielectric layer) is cleaned and spined with LOL2000 and S1805 photoresists, then patterned by ultraviolet lithography, and deposited with Cr and Au through physical vapor deposition. The photoresist is lifted off, and the pattern of Cr/Au (5 nm/50 nm) on the silicon wafer is regarded as the outer electrode (**Figure 1a,e**). The silicon wafer with outer electrode is affixed with a tiny MoS₂ nanosheet by mechanical exfoliation (**Figure 1b,f**).^[45–47] The methylmethacrylate (MMA) and polymethylmethacrylate (PMMA) photoresists are spined on the silicon wafer subsequently, which are patterned by electron-beam lithography and further deposited with Cr and Au. After lifting off the photoresist, the pattern of Cr/Au (5 nm/150 nm), which is used to contact the outer electrode and the individual MoS₂ nanosheet, is regarded as the inner electrode (**Figure 1c,g**). A layer of PMMA is spined on the silicon wafer as the passivation layer, then a window is etched by electron-beam lithography to expose the MoS₂ nanosheet (**Figure 1d,h**). The optical (**Figure 1e–h**) and scanning electron microscope (SEM) images (**Figure 2a**) show that the MoS₂ nanosheet is connected with the Cr/Au electrodes, which are fully covered by the PMMA passivation layer to avoid

J. H. Wang, Dr. M. Y. Yan, K. N. Zhao, X. B. Liao, X. L. Pan, W. Yang, Prof. L. Q. Mai
State Key Laboratory of Advanced Technology for Materials Synthesis and Processing
Wuhan University of Technology
Wuhan 430070, P. R. China
E-mail: ymymiles@whut.edu.cn; mlq518@whut.edu.cn
P. Y. Wang
Department of Mechanical and Aerospace Engineering
Monash University
Victoria 3800, Australia



DOI: 10.1002/adma.201604464

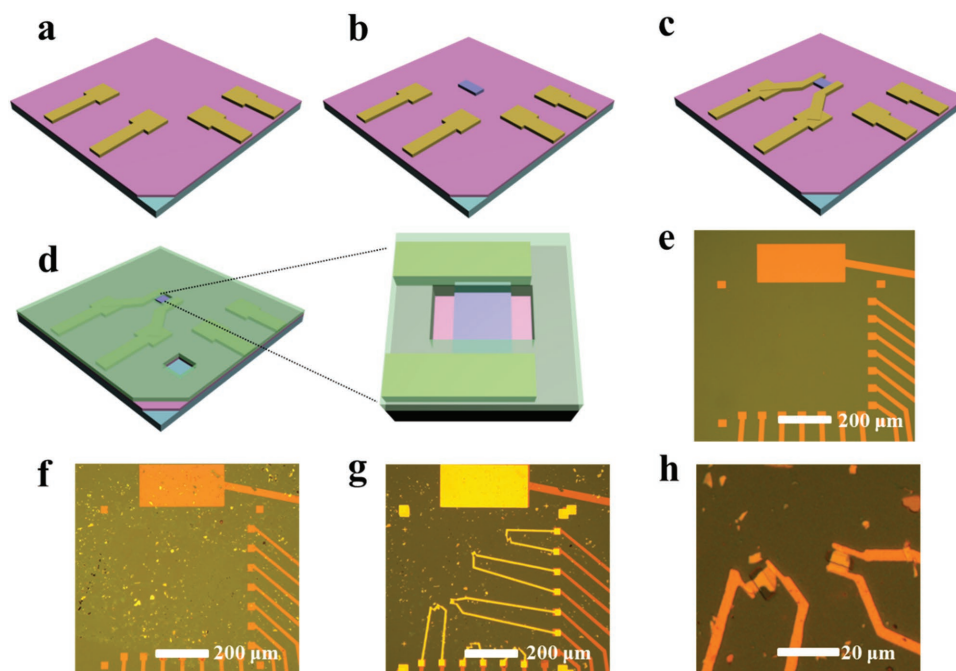


Figure 1. The 3D schematic of the field-tuned individual MoS₂ nanosheet based HER device fabrication process. a) Si substrate (blue) with 300 nm SiO₂ on the surface (pink) and showing an as-prepared 5 nm/50 nm Cr/Au (gold) outer electrode. b) An individual MoS₂ nanosheet (purple) obtained by mechanical exfoliation is transferred on the SiO₂ surface. c) The MoS₂ nanosheet is immobilized by electron-beam lithography followed by Cr/Au (5 nm/150 nm) contact deposition in a thermal evaporator. d) The photoresist (PMMA) (green) is patterned to cover over the silicon wafer with exposed MoS₂ sheets by using electron-beam lithography. The exposed high conduct silicon ($\leq 0.005 \Omega \text{ cm}^{-1}$) substrate is used to add back gate voltage. e–h) The optical image of individual MoS₂ nanosheet based HER device under different fabrication phase, corresponding to the 3D view of (a–d) respectively.

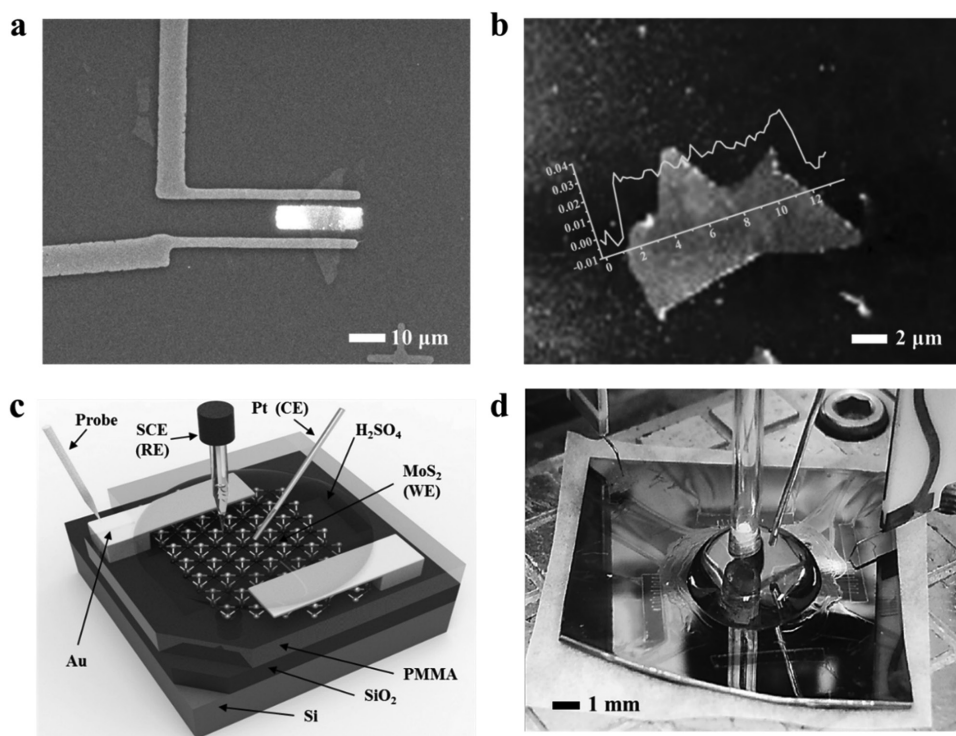


Figure 2. a) The FESEM images of an individual MoS₂ nanosheet based HER device. b) The atomic force microscopy image of the MoS₂ nanosheet. c) The schematic diagram of three electrodes for HER catalytic measurement. d) The physical connection diagram of the catalytic measurement.

the leakage current between Cr/Au electrodes and counter electrode. The atomic force microscope (AFM) images of the device (Figure 2b) show that the thickness of MoS₂ nanosheet is averagely 25 nm.

Catalytic performance of the individual MoS₂ nanosheet based HER device was measured by three electrodes system, which is in accordance with typical HER catalysis measurement.^[48,49] Figure 2c is the schematic diagram of three electrodes: an MoS₂ nanosheet acts as the working electrode, a saturated calomel electrode (SCE) is used as reference electrode, and a Pt filament with the diameter of 0.5 mm is used as the counter electrode. The connection diagram has been shown in the Figure 2d that all the three electrodes are immersed in 0.5 M H₂SO₄ electrolyte and a probe connected with an exposed high conduct silicon ($\leq 0.005 \Omega \text{ cm}^{-1}$) substrate as the source of gate voltages. Linear sweep voltammetry with a scan rate of 5 mV s⁻¹ is used to test the polarization curve of HER.

The catalytic performance of individual MoS₂ nanosheet based HER device has been investigated under different electric field intensities. In order to ensure the accuracy of the experiment, the blank control group of the same HER device without MoS₂ nanosheet (SEM image as Figure S2 in the Supporting Information) has also been fabricated and measured. Besides, the catalytic performance of Au and Pt filament (replace MoS₂ nanosheet as the working electrode) under the same condition have also been researched to compare with that of MoS₂ nanosheet (without gate voltage; Figure 3a). No obvious catalytic phenomenon is observed in the blank control group, and

the overpotentials of Pt, Au, and MoS₂ are 25, 500, and 240 mV, respectively. At the same time, the conductances of blank sample, PMMA, MoS₂ nanosheet, and Au are also measured (Figure S3, Supporting Information). Blank sample and PMMA are insulated, and the current in *I*-*V* curve of Au is almost four orders of magnitude larger than that of MoS₂. Results of catalysis and conductance sufficiently certify that the Au electrode passivated with PMMA does not partake in catalysis and the polarization current fully considered as catalytic current of MoS₂ is reasonable. The Raman peaks of MoS₂ and silicon can be found in the Raman spectra (Figure 3b).^[50-52] After catalytic test, no obvious Raman peak shift can be observed. The reduction of Raman peak intensity indicates that a slight degradation of MoS₂ crystal structure existed in the catalytic reaction. Energy dispersive spectrometry (EDS) element mapping images (Figure S4, Supporting Information) demonstrate that the morphology and element component of individual MoS₂ nanosheet remains unchanged after the HER catalysis measurement.

The polarization curves of the individual MoS₂ nanosheet based HER device at different gate voltages are shown in Figure 3c; the catalytic property has been largely boosted with the increasing of gate voltage. The overpotential of different gate voltages has been calculated at the catalytic current density of 100 mA cm⁻² and shown in Table S1 in the Supporting Information. A relative low overpotential (38 mV) is achieved with the current density of 100 mA cm⁻² at the gate voltage of 5 V, which is much lower than that without gate voltage

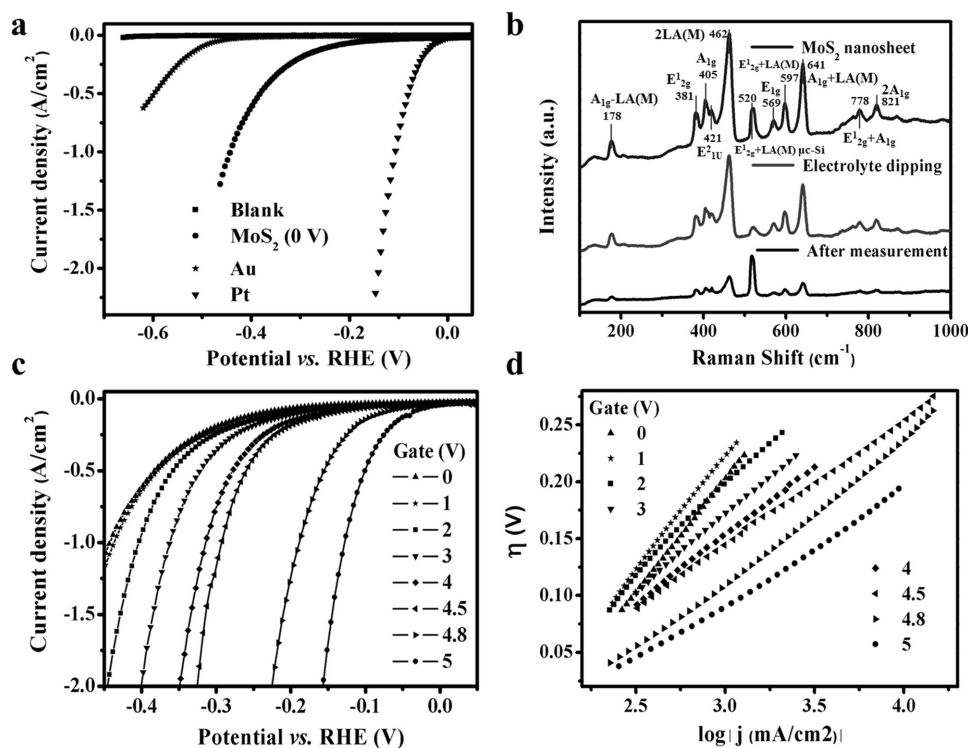


Figure 3. a) The HER polarization curves of blank sample, Au electrode, MoS₂ nanosheet, and Pt. b) Raman spectra of the primary MoS₂ nanosheet, MoS₂ nanosheet after electrolyte dipping, and the individual MoS₂ nanosheet after electrochemical measurement. c) The polarization curves of HER at different back gate voltages. The best catalytic performance appears at the gate voltage of 5 V. d) The corresponding Tafel curves at different gate voltages.

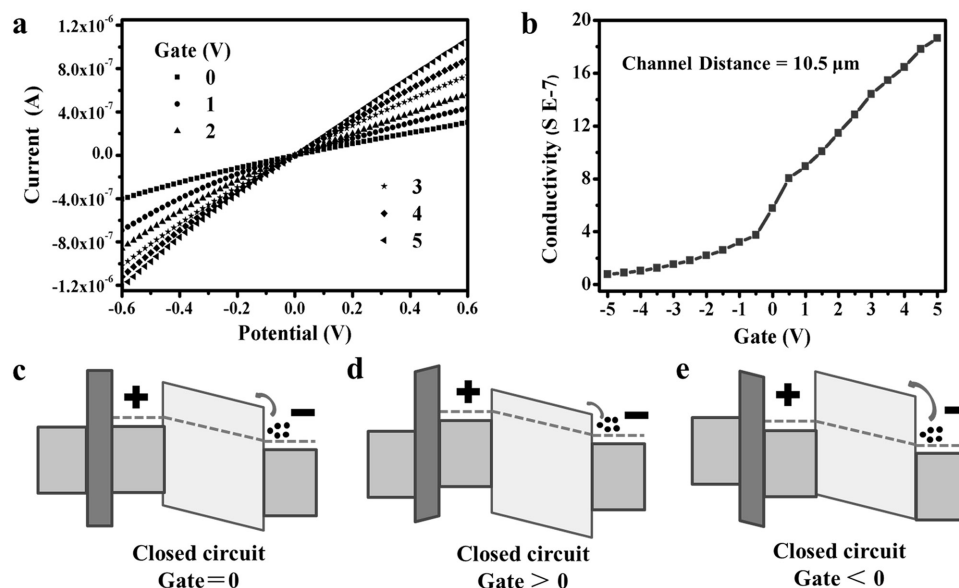


Figure 4. a) I - V curves of an individual MoS₂ nanosheet based HER device at different gate voltages, the range from 0 to 10 V. b) The channel conductance variation trend chart of the individual MoS₂ nanosheet based HER device. The energy band of the individual MoS₂ nanosheet based HER device changes with different gate voltages bias. c) The normal state of device under closed circuit without any gate voltage. d) The energy band of the device with the positive gate voltage bias, e) with the negative gate voltage bias.

(240 mV). The Figure 3e and Table S2 in the Supporting Information show the Tafel curves and the corresponding value at different gate voltages, respectively. With the gate voltages increasing from 0 to 5 V, the Tafel slope decreases from 200 to 110 mV dec⁻¹. The theory from Butler-Volmer has demonstrated that the limiting Tafel slope of slow discharge reaction should be 116 mV dec⁻¹.^[12,53,54] The mediocre value of the Tafel slope implies that charge transport is the control step of the total HER catalysis reaction. Thus, the variation of electrical transport induced by field effect may be the origin of the greatly enhanced catalytic performance of MoS₂.

In order to verify our supposition, the I - V curves of the individual MoS₂ nanosheet device at different gate voltages with or without electrolyte have been tested (Figure 4a and Figure S5 in the Supporting Information). It is found that the channel conductance of individual MoS₂ nanosheet device keeps rising from 0.0073 to 0.1776 S m⁻¹ when increasing the gate voltage from -5 to 5 V (Figure 4b and Table S3, Supporting Information). And the sharper ascent tendency of the channel conductance between 0 and 5 V is more beneficial to the catalysis. The current in I - V curve and overall catalytic current of the constant bias voltage of -0.5 V are also compared in Figure S6 in the Supporting Information. The same orders of magnitude and the same variation trends demonstrate that the enhanced channel conductance is significant enough to improve the catalytic performance. Furtherly, the $I_d - V_g$ curves of both the back gate and the solution gate have been measured and shown in Figure S7 in the Supporting Information. The $I_d - V_g$ curve of the solution gate changes little with the increasing of gate voltage, while the $I_d - V_g$ curve variation of back gate is obviously higher than that of solution gate. So, the solution gate from the counter electrode will hardly influence the whole electrochemical catalytic reaction.

Here, the energy band diagram of the device is introduced to understand the variety of channel conductance. In the individual MoS₂ nanosheet based HER device, SiO₂ layer between the Si layer and MoS₂ is used as the dielectric layer, and the gate voltage probe is connected with Si layer to provide a vertical electric field where the MoS₂ nanosheet is immersed in and can be tuned. Similar with the MoS₂ transistor, Fermi level of n-type MoS₂ nanosheet close to the bottom of conduction band with the addition of positive electric field, and that facilitates the electron transfer.^[55,56] The Fermi level can be considered locating at a moderate position without gate voltage, shown in the Figure 4c, that means a high energy barrier of electron transport exists between Au and MoS₂ nanosheet. The position of Fermi level will be closer to the bottom of conduction band by adding a positive gate voltage to reduce energy barrier and then the electrical conductance increase (Figure 4d). In the opposite side, the energy barrier will be higher with a negative gate voltage (Figure 4e). The above theory analytics of energy band is agreed with the actual evolution of channel conductance with different gate voltage. The faster electron transport is achieved with the positive gate voltage, which results in a great drop of overpotential and decreased Tafel slope.

We have successfully fabricated the individual MoS₂ nanosheet based HER device, and furthermore an electric field has been applied to explore the influence of field effect on the catalytic performance of individual MoS₂ nanosheet. It is demonstrated that HER performance of individual MoS₂ nanosheet can be further improved by adding a positive electric field. With adding a gate voltage of 5 V, the catalytic overpotential of MoS₂ decreases from 240 to 38 mV, which is comparable to that of Pt. The outstanding performance is mainly contributed from the increased channel conductance of MoS₂ nanosheet based HER

device, which is understood through the energy band theory. Such strategy of utilizing the electric field to improve the catalysis of HER could also be used in the other electrochemical processes.

Experimental Section

Fabrication of the Individual MoS₂ Nanosheet Based HER Device: A suitable size silicon wafer (with 300 nm dielectric layer) was cleaned and spined with photoresist LOL2000 and S1805. Then, the prepared silicon wafer was patterned by ultraviolet lithography and deposited with Cr/Au (5 nm/50 nm) by physical vapor deposition. The photoresist was lifted off and a tiny nanosheet of MoS₂ was transported to the silicon wafer by mechanical exfoliation of bulk MoS₂. The silicon wafer was spined with a MMA and PMMA photoresist, patterned by electron-beam lithography, and deposited with Cr/Au (5 nm/150 nm). After lifting off the photoresist, a new layer of PMMA was spined on the silicon wafer as the passivation layer, in which a groove was etched by electron-beam lithography to expose the MoS₂ nanosheet.

Electronic Conductance and Electrochemical Measurements: The probe station and semiconductor device analyzer were used to measure the electrical transport characteristics of the MoS₂ nanosheet at a series of back gate voltages. The electrochemical performance of the MoS₂ nanosheet was further tested by combining electrochemical workstation (giving/testing the signal of electrochemical reaction), probe station, and semiconductor device analyzer (giving the back gate voltage). Catalytic performance of the individual MoS₂ nanosheet based HER device were measured by a three electrodes system with the individual MoS₂ nanosheet as the working electrode, a SCE as the reference electrode, and a Pt filament with a diameter of 0.5 mm as the count electrode. All these three electrodes were immersed in 0.5 M H₂SO₄ electrolyte. A probe, which connected the exposed high conduct silicon ($\leq 0.005 \Omega \text{ cm}^{-1}$) substrate and the semiconductor device analyzer, was used as the source of the gate voltages. The polarization curve of HER was measured through linear sweep voltammetry at a scan rate of 5 mV s⁻¹.

Characterization Instrumentation: SEM imaging, EDS element mapping and electron-beam lithography were realized with a JEOL-7100F microscopy. Raman spectra were obtained using a Renishaw INVIA micro-Raman spectroscopy system. Linear sweep voltammetry of catalysis was measured by a probe station (Lake shore, PPT4), an electrochemical workstation (Autolab PGSTAT 302N), and a semiconductor device analyzer (Agilent, B1500A).

Supporting Information

Supporting Information is available from the Wiley Online Library or from the author.

Acknowledgements

This work was supported by the National Key Research Program of China (2016YFA0202603), the National Basic Research Program of China (2013CB934103), the National Natural Science Foundation of China (51521001, 51272197), the National Natural Science Fund for Distinguished Young Scholars (51425204), the Hubei Provincial Natural Science Fund for Distinguished Young Scholars (2014CFA035), and the Fundamental Research Funds for the Central Universities (WUT: 2015-PY-2, 2016111001).

Received: August 22, 2016
Revised: November 3, 2016
Published online:

- [1] J. M. Bockris, in *Environmental Chemistry*, (Ed: J. M. Bockris), Springer, NY **1977**, pp. 549–582.
- [2] M. S. Dresselhaus, I. L. Thomas, *Nature* **2001**, *414*, 332.
- [3] M. Grätzel, *Nature* **2001**, *414*, 338.
- [4] N. S. Lewis, D. G. Nocera, *Proc. Natl. Acad. Sci. USA* **2006**, *103*, 15729.
- [5] G. W. Crabtree, M. S. Dresselhaus, M. V. Buchanan, *Phys. Today* **2004**, *57*, 39.
- [6] Y. Tachibana, L. Vayssieres, J. R. Durrant, *Nat. Photonics* **2012**, *6*, 511.
- [7] L. A. Kibler, *ChemPhysChem* **2006**, *7*, 985.
- [8] M. G. Walter, E. L. Warren, J. R. McKone, S. W. Boettcher, Q. Mi, E. A. Santori, N. S. Lewis, *Chem. Rev.* **2010**, *110*, 6446.
- [9] X. Zhang, Z. Lai, C. Tan, H. Zhang, *Angew. Chem. Int. Ed.* **2016**, *55*, 8816.
- [10] Q. Lu, Y. Yu, Q. Ma, B. Chen, H. Zhang, *Adv. Mater.* **2016**, *28*, 1917.
- [11] C. Tan, H. Zhang, *Chem. Soc. Rev.* **2015**, *44*, 2713.
- [12] C. G. Morales-Guio, L. A. Stern, X. Hu, *Chem. Soc. Rev.* **2014**, *43*, 6555.
- [13] Y. Sun, S. Gao, F. Lei, Y. Xie, *Chem. Soc. Rev.* **2015**, *44*, 623.
- [14] W. Sheng, H. A. Gasteiger, Y. Shao-Horn, *J. Electrochem. Soc.* **2010**, *157*, B1529.
- [15] J. K. Norskov, C. H. Christensen, *Science* **2006**, *312*, 1322.
- [16] J. Greeley, T. F. Jaramillo, J. Bonde, I. B. Chorkendorff, J. K. Norskov, *Nat. Mater.* **2006**, *5*, 909.
- [17] J. D. Benck, T. R. Hellstern, J. Kibsgaard, P. Chakthranont, T. F. Jaramillo, *ACS Catal.* **2014**, *4*, 3957.
- [18] M. S. Faber, S. Jin, *Energy Environ. Sci.* **2014**, *7*, 3519.
- [19] X. Huang, Z. Zeng, H. Zhang, *Chem. Soc. Rev.* **2013**, *42*, 1934.
- [20] R. Chianelli, A. Ruppert, S. Behal, B. Kear, A. Wold, R. Kershaw, *J. Catal.* **1985**, *92*, 56.
- [21] T. F. Jaramillo, K. P. Jørgensen, J. Bonde, J. H. Nielsen, S. Horch, I. Chorkendorff, *Science* **2007**, *317*, 100.
- [22] H. I. Karunadasa, E. Montalvo, Y. Sun, M. Majda, J. R. Long, C. J. Chang, *Science* **2012**, *335*, 698.
- [23] J. Xie, Y. Xie, *ChemCatChem* **2015**, *7*, 2568.
- [24] H. Zhang, *ACS Nano* **2015**, *9*, 9451.
- [25] M. A. Lukowski, A. S. Daniel, F. Meng, A. Forticaux, L. Li, S. Jin, *J. Am. Chem. Soc.* **2013**, *135*, 10274.
- [26] J. Kibsgaard, Z. Chen, B. N. Reinecke, T. F. Jaramillo, *Nat. Mater.* **2012**, *11*, 963.
- [27] Z. Lu, W. Zhu, X. Yu, H. Zhang, Y. Li, X. Sun, X. Wang, H. Wang, J. Wang, J. Luo, X. Lei, L. Jiang, *Adv. Mater.* **2014**, *26*, 2683.
- [28] J. Ding, Y. Zhou, Y. Li, S. Guo, X. Huang, *Chem. Mater.* **2016**, *28*, 2074.
- [29] D. Merki, H. Vrubel, L. Rovelli, S. Fierro, X. Hu, *Chem. Sci.* **2012**, *3*, 2515.
- [30] L. Tao, X. Duan, C. Wang, X. Duan, S. Wang, *Chem. Commun.* **2015**, *51*, 7470.
- [31] J. Xie, H. Zhang, S. Li, R. Wang, X. Sun, M. Zhou, J. Zhou, X. W. Lou, Y. Xie, *Adv. Mater.* **2013**, *25*, 5807.
- [32] J. Xie, J. Zhang, S. Li, F. Grote, X. Zhang, H. Zhang, R. Wang, Y. Lei, B. Pan, Y. Xie, *J. Am. Chem. Soc.* **2013**, *135*, 17881.
- [33] Y. Li, H. Wang, L. Xie, Y. Liang, G. Hong, H. Dai, *J. Am. Chem. Soc.* **2011**, *133*, 7296.
- [34] Y. Shi, J. Wang, C. Wang, T. T. Zhai, W. J. Bao, J. J. Xu, X. H. Xia, H. Y. Chen, *J. Am. Chem. Soc.* **2015**, *137*, 7365.
- [35] L. Liao, J. Zhu, X. Bian, L. Zhu, M. D. Scanlon, H. H. Girault, B. Liu, *Adv. Funct. Mater.* **2013**, *23*, 5326.
- [36] J. Chen, X. J. Wu, L. Yin, B. Li, X. Hong, Z. Fan, B. Chen, C. Xue, H. Zhang, *Angew. Chem. Int. Ed.* **2015**, *54*, 1210.
- [37] X. Huang, Z. Zeng, S. Bao, M. Wang, X. Qi, Z. Fan, H. Zhang, *Nat. Commun.* **2013**, *4*, 1444.
- [38] Z. Zeng, C. Tan, X. Huang, S. Bao, H. Zhang, *Energy Environ. Sci.* **2014**, *7*, 797.

- [39] Z. Yin, B. Chen, M. Bosman, X. Cao, J. Chen, B. Zheng, H. Zhang, *Small* **2014**, *10*, 3537.
- [40] D. Voiry, R. Fullon, J. Yang, E. S. C. de Carvalho Castro, R. Kappera, I. Bozkurt, D. Kaplan, M. J. Lagos, P. E. Batson, G. Gupta, A. D. Mohite, L. Dong, D. Er, V. B. Shenoy, T. Asefa, M. Chhowalla, *Nat. Mater.* **2016**, *15*, 1003.
- [41] R. Kappera, D. Voiry, S. E. Yalcin, B. Branch, G. Gupta, A. D. Mohite, M. Chhowalla, *Nat. Mater.* **2014**, *13*, 1128.
- [42] Y. Du, H. Liu, A. T. Neal, M. Si, D. Y. Peide, *IEEE Electron Device Lett.* **2013**, *34*, 1328.
- [43] F. Patolsky, G. Zheng, C. M. Lieber, *Nat. Protoc.* **2006**, *1*, 1711.
- [44] L. Mai, Y. Dong, L. Xu, C. Han, *Nano Lett.* **2010**, *10*, 4273.
- [45] C. Berger, Z. Song, T. Li, X. Li, A. Y. Ogbazghi, R. Feng, Z. Dai, A. N. Marchenkov, E. H. Conrad, P. N. First, W. A. de Heer, *J. Phys. Chem. B* **2004**, *108*, 19912.
- [46] K. S. Novoselov, A. K. Geim, S. V. Morozov, D. Jiang, Y. Zhang, S. V. Dubonos, I. V. Grigorieva, A. A. Firsov, *Science* **2004**, *306*, 666.
- [47] K. S. Novoselov, D. Jiang, F. Schedin, T. J. Booth, V. V. Khotkevich, S. V. Morozov, A. K. Geim, *Proc. Natl. Acad. Sci. USA* **2005**, *102*, 10451.
- [48] H. Lv, Z. Xi, Z. Chen, S. Guo, Y. Yu, W. Zhu, Q. Li, X. Zhang, M. Pan, G. Lu, S. Mu, S. Sun, *J. Am. Chem. Soc.* **2015**, *137*, 5859.
- [49] D. Y. Wang, M. Gong, H. L. Chou, C. J. Pan, H. A. Chen, Y. Wu, M. C. Lin, M. Guan, J. Yang, C. W. Chen, Y. L. Wang, B. J. Hwang, C. C. Chen, H. Dai, *J. Am. Chem. Soc.* **2015**, *137*, 1587.
- [50] B. C. Windom, W. G. Sawyer, D. W. Hahn, *Tribol. Lett.* **2011**, *42*, 301.
- [51] H. Richter, Z. Wang, L. Ley, *Solid State Commun.* **1981**, *39*, 625.
- [52] J. M. Chen, C. S. Wang, *Solid State Commun.* **1974**, *14*, 857.
- [53] J. O. M. Bockris, E. C. Potter, *J. Electrochem. Soc.* **1952**, *99*, 169.
- [54] S. Fletcher, *J. Solid State Electrochem.* **2009**, *13*, 537.
- [55] Z. Yin, H. Li, H. Li, L. Jiang, Y. Shi, Y. Sun, G. Lu, Q. Zhang, X. Chen, H. Zhang, *ACS Nano* **2012**, *6*, 74.
- [56] S. Kim, A. Konar, W. S. Hwang, J. H. Lee, J. Lee, J. Yang, C. Jung, H. Kim, J. B. Yoo, J. Y. Choi, Y. W. Jin, S. Y. Lee, D. Jena, W. Choi, K. Kim, *Nat. Commun.* **2012**, *3*, 1011.